Transition Metal Chemistry
https://doi.org/10.1007/s11243-021-00460-w

Selective oxidation of benzyl alcohols to benzaldehydes catalyzed by dioxomolybdenum Schiff base complex: synthesis, spectral characterization, crystal structure, theoretical and computational studies

Hadi Kargar[1] · Mehdi Fallah-Mehrjardi[2] · Reza Behjatmanesh-Ardakani[2] · Khurram Shahzad Munawar[3,4] · Muhammad Ashfaq[5] · Muhammad Nawaz Tahir[5]

Received: 12 February 2021 / Accepted: 24 April 2021

Abstract
A novel dioxomolybdenum Schiff base complex, MoO_2L·DMF, was synthesized by treating $MoO_2(acac)_2$ with an ONO donor Schiff base ligand (H_2L) derived by the condensation of 4-aminobenzohydrazide and 3-methoxysalicylaldehyde. The synthesized ligand and complex were characterized by physicochemical and spectroscopic techniques. Single-crystal X-ray analysis was also accomplished to ensure the molecular structure of the complex. The geometry around the central metal atom in MoO_2L·DMF was distorted octahedral as revealed by the data collected from diffraction studies. Theoretical calculations of the synthesized compounds were carried out by DFT at B3LYP/Def2-TZVP level of theory, which showed a good correlation with the experimental findings. Moreover, the homogeneous catalytic efficiency of the complex was investigated by the process of selective oxidation of benzylic alcohols using urea hydrogen peroxide (UHP) in acetonitrile under reflux conditions.

Introduction

Selective oxidation of organic compounds to get valuable products is getting much more attention day by day. These reactions are very important from an industrial perspective for the production of oxygenated species [1]. The organic transformations are very slow and require a lot of time to complete. Finally, it becomes very costly and unaffordable to get the desired products from an economical point of view. Hence, the use of transition metals as homogeneous or heterogeneous catalysts in selective oxidation processes is becoming an important area of research in organic synthesis [2]. A very important and basic reaction at both laboratory and industrial scale is the partial oxidation of alcohols to their respective aldehydes and ketones [3]. For this, dozens of protocols have been invented by utilizing a variety of organic and inorganic reagents to attain the particular products [4].

Hydrazone-based Schiff bases establish a distinctive class of ligands with N- and O-atoms as donor sites. These Schiff bases, obtained by the treatment of aromatic acid hydrazides with the derivatives of salicylaldehydes, have high propensity to fabricate transition metal complexes [5]. These aroyl hydrazones can coordinate to the metal center in a tridentate fashion via iminic nitrogen of hydrazone part, amide oxygen atom and deprotonated ortho hydroxyl group [6]. Hydrazones can hold the transition metals in their highest oxidation states which give a plus point to their suitability to tolerate different reaction conditions for catalytic transformations [7].

Molybdenum is referred to as one of the very attractive and useful transition metals in industrial as well as

✉ Hadi Kargar
h.kargar@ardakan.ac.ir; hadi_kargar@yahoo.com

1 Department of Chemical Engineering, Faculty of Engineering, Ardakan University, P.O. Box 184, Ardakan, Iran

2 Department of Chemistry, Payame Noor University, 19395-3697 Tehran, Iran

3 Department of Chemistry, University of Sargodha, Punjab, Pakistan

4 Department of Chemistry, University of Mianwali, Mianwali, Pakistan

5 Department of Physics, University of Sargodha, Punjab, Pakistan

Published online: 06 May 2021

in biochemical processes [8]. The dioxomolybdenum(VI) salt of acetylacetonate, utilized in numerous substitution reactions, is denoted as a very important molecular catalyst for homogeneous epoxidation of olefins [9]. The dioxomolybdenum(VI) complexes have been investigated expansively due to their key role in oxo-transfer reactions [4, 9]. Owing to their outstanding importance in enzymatic reactions in biological processes [10], particularly in oxidation of aldehydes, sulfides and purines [11], plenty of dioxomolybdenum complexes were synthesized to investigate their oxygen transfer features [4, 9, 12].

There are different kinds of compounds which are utilized as a source of oxygen but UHP is preferred over rest of these because of high oxygen content, easy operating procedure, inexpensive and environmentally friendly nature [13]. UHP usually reacts with metals to produce an active metal catalyst with a peroxy ligand (MOOR), which eventually shifts an O center to the substrate [14]. Among the catalysts which are metal based, the Mo containing complexes proved themselves to have potential for their utilization as effective catalysts for oxidation reactions in the presence of peroxides [4].

Although, quite a few dioxomolybdenum(VI) compounds are effectively being utilized in numerous oxidation reactions [15] but still there are very inadequate number of findings about the employing these complexes for the oxidation of alcohols into aldehydes and ketones [16]. Another important aspect of the modern era is the involvement of computational chemistry for theoretical calculations like density functional theory (DFT) to find out the molecular properties [17].

Getting motivation from remarkable properties of Mo complexes, current work is focused on the synthesis of dioxomolybdenum(VI) complex with hydrazone-based Schiff base ligand and its utilization as an effective catalyst for selective oxidation of benzylic alcohols and then conduction of their experimental and theoretical findings to explore their structural features.

Experimental

Materials and methods

All the chemicals employed in the current work were 99.9% pure and purchased from well-renowned suppliers like Sigma-Aldrich and Merck. The C, H and N microanalyses of the crystalline products were obtained with a Heraeus CHN–O–FLASH EA 1112 elemental analyzer. ^{1}H and ^{13}C NMR spectra of the powdered samples were measured at ambient temperature by using BRUKER AVANCE 400 MHz spectrometer by employing tetramethylsilane (TMS) as internal reference and dimethyl sulfoxide (DMSO-d_6) as solvent. Coupling constant (J) and chemical shift (δ) values were reported in Hz and in ppm, respectively. Infrared spectra of the crystalline compounds were taken by making KBr disks on a Shimadzu FTIR IRPrestige-21 spectrophotometer.

Synthesis of H_2L

4-aminobenzohydrazide (1.51 g, 10 mmol) and 3-methoxysalicylaldehyde (1.52 g, 10 mmol) were dissolved separately in hot methanol (25 mL). After complete dissolution, both solutions were mixed dropwise with continuous stirring. The resulting mixture was refluxed for approximately 3 h until the reaction was completed which was ensured by continuous monitoring with the help of TLC. On allowing the reaction mixture to attain the room temperature, the product was settled down leaving behind the impurities in the solvent. Finally, the desired product was collected by filtration, aided by suction apparatus and washed thrice with cold methanol to remove impurities if any.

H_2L: Yield 0.23 g (81%). Anal. calcd. for $C_{15}H_{15}N_3O_3$ (%): C, 63.2; H, 5.3; N, 14.7. Found: C, 63.3; H, 5.4; N, 14.6. FTIR (KBr, cm^{-1}); 3624 (ν_{N-H}); 1639 ($\nu_{C=O}$); 1602 ($\nu_{C=N}$); 1475, 1556 ($\nu_{C=C}$); 1269 (ν_{C-O}); 1085 (ν_{N-N}). ^{1}H NMR (400 MHz DMSO-d_6, ppm): 3.81 [3 H, s, (–OCH_3)], 5.88 [2 H, s, (–NH_2),], 6.61 [2 H, (H–C_{12}, H–C_{14}), t, ^{3}J = 8.4 Hz], 6.88 [1 H, (H–C_4), t, ^{3}J = 8.0 Hz], 7.02 [1 H, (H–C_3), dd, ^{3}J = 8.0 Hz, ^{4}J = 1.2 Hz], 7.07 [1 H, (H–C_5), dd, ^{3}J = 8.0 Hz, ^{4}J = 1.2 Hz], 7.68 [2 H, (H–C_{11}, H–C_{15}), d, ^{3}J = 8.4 Hz], 8.56 [1 H, s, (–CH=N),], 11.33 [1 H, s, (–NH)], 11.73 [1 H, s, (–OH)]. ^{13}C NMR (100 MHz, DMSO-d_6, ppm): 55.7 (C_7), 112.7 (C_{12}, C_{14}), 113.5 (C_3), 118.7 (C_4), 119.0 (C_6), 121.0 (C_{10}), 121.3 (C_5), 129.4 (C_{11}, C_{15}), 146.8 (C_8), 147.0 (C_2), 147.8 (C_1), 152.4 (C_{13}), 162.7 (C_9).

Synthesis of $Mo^{VI}O_2L$·DMF

Equimolar amounts of H_2L (0.285 g, 1 mmol) and $MoO_2(acac)_2$ (0.330 g, 1 mmol) were suspended in methanol (100 mL) with continuous stirring to attain the uniformity. The suspension was refluxed for about 3 h and then 2/3rd of the solvent was evaporated to concentrate the mixture and the remaining solution was cooled over an ice bath to get the orange-colored product. These precipitates were dissolved in minimum amount of DMF to get the pure crystalline product suitable for single-crystal X-ray analysis. The crystals were collected by filtration and then washed carefully with water, methanol and diethyl ether, separately, and finally dried in *vacuo*.

MoO_2L·DMF: Yield 0.35 g (73%) (Powdered sample). Anal. calcd. for $C_{18}H_{20}MoN_4O_6$ (%): C, 44.6; H, 4.2; N, 11.6. Found: C, 44.8; H, 4.2; N, 11.4. FTIR (KBr, cm^{-1}); 1651 ($\nu_{C=Odmf}$); 1604 ($\nu_{C=N}$); 1465 ($\nu_{C=N-N=C}$); 1436, 1544 ($\nu_{C=C}$); 1346 ($\nu_{C\text{-}Oenolate}$); 1261 ($\nu_{C\text{-}Ophenolate}$); 1014 ($\nu_{N-N}$); 935 ($\nu_{O=Mo=O}$) *asym*; 912 ($\nu_{O=Mo=O}$) *sym*; 898, 831

($\nu_{O=Mo\text{-}Odmf}$), 590 (ν_{Mo-O}); 466 (ν_{Mo-N}). ^{1}H NMR (400 MHz, DMSO-d_6, ppm): 3.80 [3 H, *s*, (–OCH_3], 5.96 [2 H, *s*, (–NH_2),], 6.60 [2 H, (H–C_{12}, H–C_{14}), *t*, $^{3}J = 8.4$ Hz], 6.99 [1 H, (H–C_4), t, $^{3}J = 8.0$ Hz], 7.19 [1 H, (H–C_3), *d*, $^{3}J = 8.0$ Hz], 7.25 [1 H, (H–C_5), *d*, $^{3}J = 8.0$ Hz], 7.68 [2 H, (H–C_{11}, H–C_{15}), *d*, $^{3}J = 8.4$ Hz], 8.76 [1 H, *s*, (–CH=N),]. ^{13}C NMR (100 MHz, DMSO-d_6, ppm): 55.7 (C_7) 113.1 (C_{12}, C_{14}), 115.6 (C_3), 116.2 (C_4), 120.8 (C_6), 121.2 (C_{10}), 124.7 (C_5), 129.9 (C_{11}, C_{15}), 148.4 (C_1), 148.8 (C_2), 152.6 (C_{13}), 153.0 (C_8), 169.4 (C_9).

X-ray crystallographic data collection and structural determination of complex

Diffractometer, named as Bruker Kappa APEX-II CCD, is employed for the data collection of MoO_2L·DMF equipped with an X-rays source in which the target is made up of molybdenum. X-rays are monochromated with the help of graphite-based monochromators to generate Mo–Kα radiations. APEX-II software [18] is employed for data collection and the absorption correction is performed by using ω-scan method in SADABS [19] software. Raw data are solved by employing a direct method in SHELXL-97 [20] software. Data refinement is performed by employing the full-matrix least-squares method on F2 in SHELXL [21] software. All the atoms are refined using anisotropic displacement parameters except H-atoms. H-atoms are placed at ideal positions by employing relative isotropic displacement parameters. For the sake of graphical representation of X-rays analysis results, ORTEP-3 [22], PLATON [23] and Mercury [24] software are employed. Experimental features related to X-ray's analysis of MoO_2L·DMF are specified in Table 1.

Table 1 Crystal data and refinement parameters for MoO_2L·DMF complex

Empirical formula	$C_{18}H_{20}MoN_4O_6$
Formula weight	484.32
Temperature/K	296
Crystal system	Monoclinic
Space group	$P2_1/c$
a/Å	17.3348(12)
b/Å	8.5257(6)
c/Å	13.9484(9)
α/°	90
β/°	93.650(2)
γ/°	90
Volume/Å^3	2057.3(2)
Z	4
ρ_{calc} (mg/mm^3)	1.564
μ (mm^{-1})	0.679
Crystal size (mm)	0.25 × 0.16 × 0.15
F(000)	984
θ range for data collection	1.177° to 25.989°
Index ranges	$-21 \le h \le 21, -9 \le k \le 10, -17 \le l \le 15$
$(\sin\theta/\lambda)_{max}$ (Å^{-1})	0.617
No. of measured, independent and observed [$I > 2\sigma(I)$] reflections	14,378, 4019, 3351
Data/restraints/parameters	4019/78/295
R(int)	0.044
$R[F^2 > 2\sigma(F^2)]$, $wR(F^2)$, *S*	0.067, 0.173, 1.23
H-atom treatment	H-atoms are treated by a mixture of independent and constrained refinements
$\Delta\rho_{max}$, $\Delta\rho_{min}$(e Å^{-3})	2.42, – 1.51

Computational details

Density functional theory (DFT) calculations were performed with the Gaussian 09 package [25] at B3LYP level of theory [26] by using Def2-TZVP basis set [27]. The solution phase was modeled by using IEFPCM with the consideration of solvent [28]. Geometry optimizations were tested by frequency analysis to ensure that they are at the local minima on the molecular potential energy surface (PES). The results showed that there is no imaginary frequency. The ^{1}H and ^{13}C NMR magnetic isotropic shielding tensors were calculated by the standard Gauge-Independent Atomic Orbital (GIAO) approach in the solution phase [29]. Chemical shift values of compounds calculated by using B3LYP/Def2-TZVP level and IEFPCM model as an implicit model for solvent and compared with experimental data obtained in DMSO-d_6. The same solvent was used for all IEFPCM calculations for ligand, Mo complex and TMS. Chemical shifts were calculated by subtracting the appropriate isotropic part of the shielding tensor from that of TMS $\delta i = \sigma_{TMS} - \sigma_i$. The isotropic magnetic shielding tensors for TMS calculated in the solution phase at the B3LYP/Def2-TZVP level of theory were equal to 31.92 and 184.52 ppm for the ^{1}H and the ^{13}C nuclei, respectively. The Chemissian program was used to draw contour plots of highest occupied molecular orbital (HOMO) and lowest unoccupied molecular orbital (LUMO) [30].

General procedure for the selective oxidation of benzylic alcohols catalyzed by MoO_2L·DMF complex

The MoO_2L·DMF catalyst (0.006 mmol) was added to a solution of benzylic alcohol (1 mmol) and UHP (2 mmol) in CH_3CN (10 mL) and the reaction mixture was refluxed with continuous stirring for the specified intervals of times as listed in Table 10. The conversion of reactants into the products was observed continuously with the help of TLC plates by taking aliquots from reaction mixture. For this purpose,

a mixture of *n*-hexane and ethyl acetate (7:3) was employed as an eluent. On complete conversion, the resultant mixture was filtered off and then the solvent was evaporated under reduced pressure. The corresponding benzaldehydes were finally obtained in pure form with the help of column chromatography by using silica gel. All products were known compounds and also acknowledged by comparing their physicochemical characteristics, like FTIR and NMR spectra, with those of authentic samples.

Results and discussion

Synthesis

The H_2L was prepared by treating 4-aminobenzohydrazide with 3-methoxysalicylaldehyde in a methanolic environment. Reaction of $MoO_2(acac)_2$ with H_2L in methanol under reflux conditions produces the targeted molybdenum complex (Scheme 1). After successful synthesis and characterization, the catalytic effectiveness of the complex was also checked by oxidizing various benzylic alcohols using UHP as a source of oxygen (Scheme 2).

Crystal structure determination

In MoO_2L·DMF (Fig. 1, Table 1), the coordination sphere around central Mo-atom composes of phenolic O-atom (O_1), enolic O-atom (O_2) and imine N-atom (N1), from the tridentate chelating ligand, and O-atoms (O_4/O_5) of the oxo groups, and O-atom (O_6) of the coordinating dimethylformamide (DMF) solvent. The DMF acts as co-ligand to complete the coordination of the central metal atom. The ligand coordinates with the Mo-atom in a planar fashion and results in the formation of a six-membered ($Mo_1/O_1/N_1/C_1/C_6/C_8$) and a five-membered ($Mo_1/O_2/N_1/N_2/C_9$) chelating rings. Ring puckering inspection infers that a six-membered chelating ring is puckered with puckering amplitude $Q = 0.261(5)$ Å, $\theta = 115.1(15)°$ and $\varphi = 195.9(18)°$. The bond lengths and bond angles in coordination sphere are such that distorted octahedral geometry is formed as the bond angles in coordination sphere range from 71.9 (2)° to 170.1 (2)°. The selected bond lengths and bond angles are specified in Table 2. The Mo–O_6 bond length is significantly longer than other Mo–O bond lengths which gives an indication that dimethylformamide solvent is weakly bonded to Mo-atom. The equatorial sites are occupied by ($O_1/O_2/N_1$) atoms of the chelating ligand and one of the O-atom (O_4) of oxo groups. Whereas, the axial sites are occupied by the other O-atom (O_5) of oxo group and O-atom (O_6) of the coordinating dimethylformamide ligand. The central Mo-atom is deviated by 0.3143 Å from the equatorial plane defined by ($O_1/O_2/O_4/N_1$) atoms toward the Mo=O_5 moiety. The equatorial plane A ($O_1/O_2/O_4/N_1$), anisole moiety B (O_3/C_1–C_7), 1,2-dimethylhydrazine moiety C ($N_1/N_2/C_8/C_9$) and aniline group D ($/N_3C_{10}$–C_{15}) are found to be planar with respective root-mean-square (r.m.s.) deviations of 0.0003, 0.0133, 0.0004 and 0.0089 Å. Moiety C makes the respective dihedral angles of 9.77 (7)° and 4.01 (8)° with moiety B and group D. Anisole moiety B is twisted at the angle of 13.8 (4)° with respect to group D. These dihedral angle inspection infers that the whole chelating ligand is almost planar. The atoms of dimethylamine moiety E ($N_4/C_{17}/C_{18}$) of the dimethylformamide ligand ($O_6/N_4/C_{16}$–C_{18}) are disordered over two set of sites with occupancy ratio of 0.52(5): 0.48(5). The plane of the major part F ($N_4A/C_{17}A/C_{18}A$) is twisted at the dihedral angle of 15.7 (8)° with respect to the plane of minor part G ($N_4B/C_{17}B/C_{18}B$). The molecular configuration is stabilized by intramolecular C–H···O bonding and C–H···π interaction as displayed in Fig. 2 and specified in Table 2. In C–H···π interaction, CH from the dimethylformamide molecule interacts with a five-membered chelating ring of the same molecule with H···π distance of 2.89 Å. The molecules are connected with each other in the form of dimers through N_3–H_3B···O_4 bonding to form R_2^2 (20) loop as specified in Table 3 and displayed in Fig. 3. The dimers are further interlinked through N_3–H_3A···O_5 bonding. Due to N_3–H_3A···O_5, C_{11}, a zigzag chain is formed that runs along the b crystallographic axis. The molecules are also interlinked by comparatively weak H-bonding of the type C–H···O to form a C_7 chain that also runs along the b crystallographic axis. Due to abovementioned H-bonding, a 2D hydrogen bonding is formed with base vectors [010], [001] in a plane (100).

Computational and characterization

The gas phase optimized structures of the ligand and Mo(VI) complex are presented in Fig. 4. The optimized structural parameters, bond lengths and bond angles, for the MoO_2L·DMF complex obtained from DFT calculations, are listed in Table 2 along with the X-ray data. As it can be seen from Table 2 that the theoretical data are quite comparable to the experimental results. The differences between the theoretical and experimental values may be emanated from this fact that the experimental data belong to the solid state, while the calculated values describe a single molecule in the gaseous state. In accordance with X-ray crystal structures, the coordination of nitrogen and oxygen atoms to the metal center of the Mo complex in the gas phase also exhibits the distorted octahedral geometry.

The H_2L ligand deprotonates and coordinates with metal in a tridentate (N, O^-, O^-) dianionic fashion. The calculated N_1–C_8 (1.289 Å) and N_2–C_9 (1.304 Å) bond lengths are approximately close in value for a C=N double bond length. The calculated C_1–O_1 and C_9–O_3 bond lengths are 1.325 and

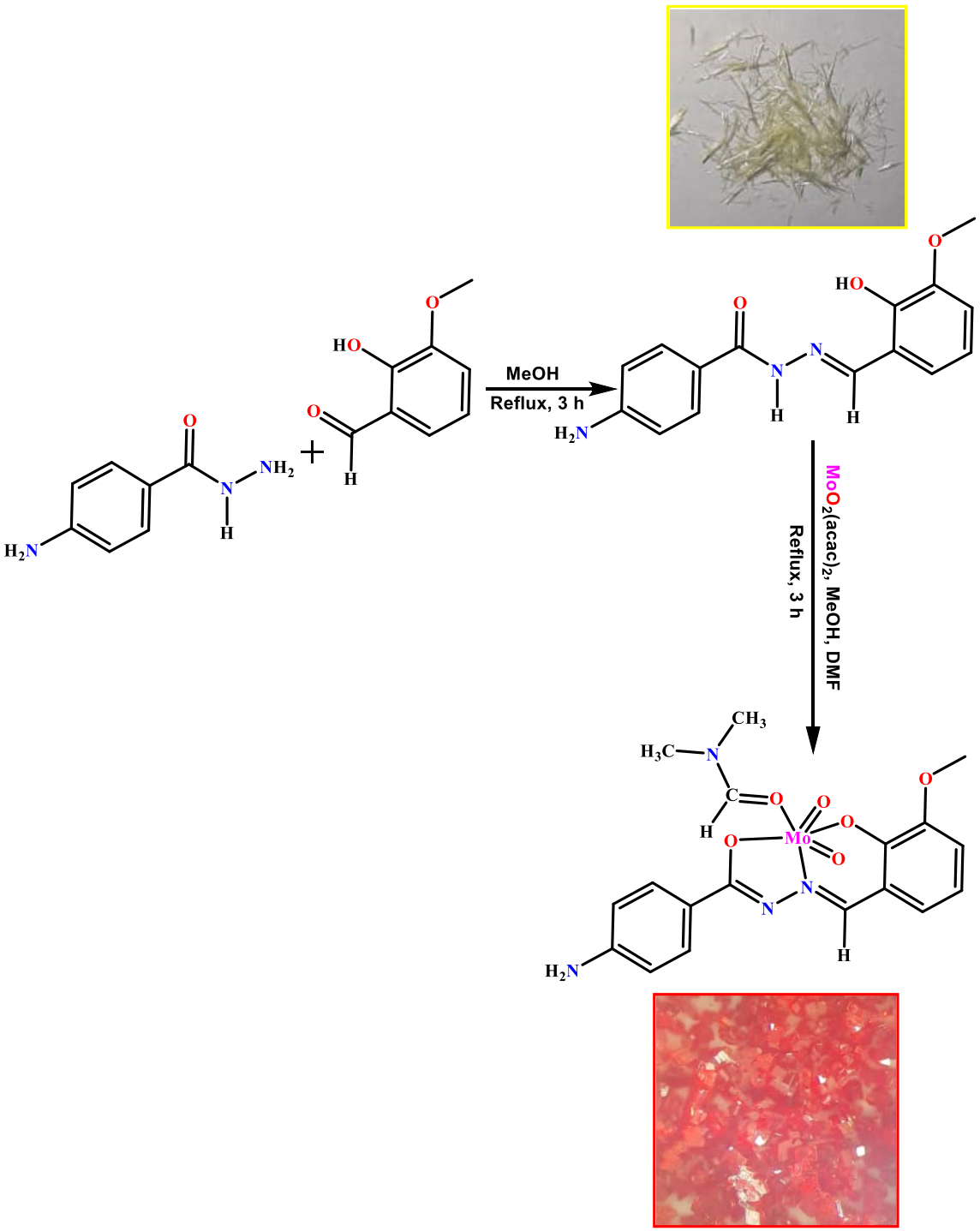

Scheme 1 Synthesis of H_2L Schiff base ligand and its $MoO_2L{\cdot}DMF$ complex

1.317 Å, respectively, which are fairly between the length of a carbon to oxygen single (C–O) (1.43 Å) and double bond (C=O) (1.21 Å). Also, the calculated bond lengths for C_6–C_8, C_1–C_6 and C_9–C_{10} are 1.440, 1.408 and 1.465 Å, respectively, which are somewhat between the length of a C–C single bond (1.54 Å) and that of a C=C double bond (1.34 Å). These values suggest that the electronic density may be delocalized on the azomethine chromophore, carbonyl groups, aromatic rings and the C_1–O_1 bond. The sum of the electronic and the zero-point energy (E^{ZPE}), enthalpy (H), and Gibbs free energy (G) of both enol and keto forms

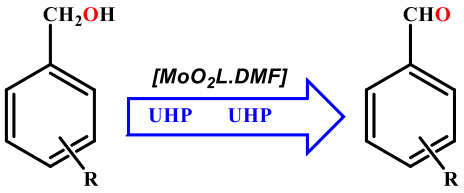

Scheme 2 Catalytic oxidation of benzylic alcohols using UHP catalyzed by $MoO_2L{\cdot}DMF$

of H_2L Schiff base ligand are reported in Table 4. Data showed that keto form is more stable in both phases.

The atomic charge on the active centers of H_2L ligand and $MoO_2L{\cdot}DMF$ complex and the amount of charge transferred from the ligand to the central metal atoms, i.e., $L \rightarrow M$ are presented in Table 5. The charge on the metal atom is considerably less than that of the formal charge (6 +) of molybdenum, which indicates that the significant amount of charge density is transferred from the ligand to the metal atom. Also, the carbon atoms (C_1 and C_9) connected to oxygen atoms (O1 and O3) have the maximum variation in the charge density after the complexation with molybdenum.

A brief overview of experimental and calculated vibrational parameters of H_2L and $MoO_2L{\cdot}DMF$ is given in Table 6. It is obvious from the data that the relative error of deviation between experimental and theoretical values is $\leq 6.18\%$. This slight divergence arises due to the application of harmonic approximation, as the calculations are performed in the vacuum.

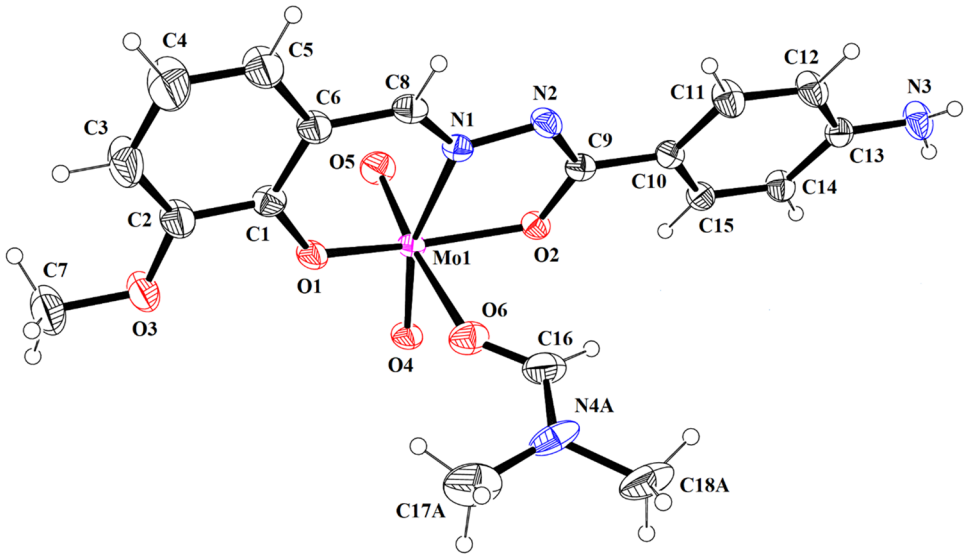

Fig. 1 ORTEP diagram of $MoO_2L{\cdot}DMF$ drawn at probability level of 30%. H-atoms are shown by small circles of arbitrary radii

Table 2 The selected experimental and calculated bond lengths (Å) and bond angles (°) of $MoO_2L{\cdot}DMF$ complex

Bond lengths	Experimental	Calculated	Bond angles	Experimental	Calculated
Mo(1)–N(1)	2.241 (6)	2.281	O(1)–Mo(1)–O(2)	150.1 (2)	146.60
Mo(1)–O(1)	1.897 (5)	1.941	O(1)–Mo(1)–O(4)	103.5 (2)	102.70
Mo(1)–O(2)	1.989 (5)	2.005	O(1)–Mo(1)–O(5)	100.2 (2)	100.41
Mo(1)–O(4)	1.707 (4)	1.706	O(1)–Mo(1)–O(6)	79.2 (2)	78.98
Mo(1)–O(5)	1.698 (6)	1.690	O(1)–Mo(1)–N(1)	82.4 (2)	78.98
Mo(1)–O(6)	2.319 (6)	2.516	O(2)–Mo(1)–O(4)	95.8 (2)	97.28
O(2)–C(9)	1.344 (8)	1.317	O(2)–Mo(1)–O(5)	96.5 (2)	98.83
N(2)–C(9)	1.303 (9)	1.304	O(2)–Mo(1)–O(6)	80.2 (2)	78.01
N(1)–C(8)	1.273 (2)	1.289	O(2)–Mo(1)–N(1)	71.9 (2)	70.60
O(1)–C(1)	1.352 (8)	1.325	O(4)–Mo(1)–O(5)	105.3 (3)	107.24
O(3)–C(2)	1.364 (2)	1.356	O(4)–Mo(1)–O(6)	84.4 (2)	81.08
C(13)–N(3)	1.358 (2)	1.383	O(4)–Mo(1)–N(1)	159.1 (2)	153.93
O(6)–C(16)	1.213 (1)	1.231	O(5)–Mo(1)–O(6)	170.1 (2)	171.49
C(16)–N_4A	1.399 (2)	1.342	O(5)–Mo(1)–N(1)	93.1 (3)	97.58
			O(5)–Mo(1)–O(6)	77.0 (2)	73.93

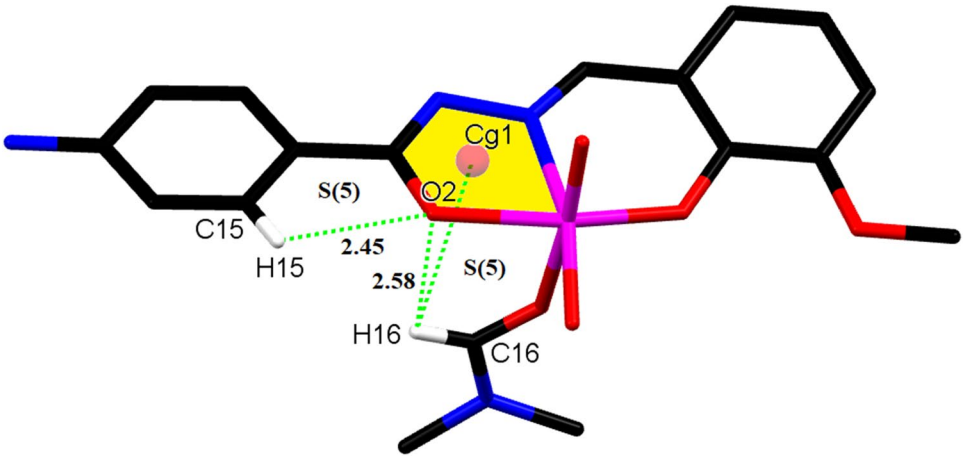

Fig. 2 Graphical representation of interactions that stabilize the molecular configuration. Distances are measured in Å. Only selected H-atoms are shown for clarity. Cg1 is a centroid of a five-membered ring ($Mo_1/O_2/N_1/N_2/C_9$)

Table 3 Hydrogen-bond geometry (Å, º) for MoO_2L·DMF

D–H···*A*	*D*–H	H···*A*	*D*···*A*	<(*D*–H···*A*)°
N_3–H_3A···O_5^{i}	0.76 (10)	2.39 (11)	3.130 (10)	168 (10)
N_3–H_3B···O_4^{ii}	0.86 (10)	2.22 (10)	3.068 (10)	170 (9)
$C_{17}A$–$H_{17}B$···O_5^{iii}	0.96	2.61	3.44 (6)	144
$C_{17}B$–$H_{17}D$···O_4^{iii}	0.96	2.65	3.46 (3)	142
$C_{17}B$–$H_{17}D$···O_5^{iii}	0.96	2.59	3.38 (5)	141
C_{15}–H_{15}···O_2	0.93	2.45	2.777	100.94
C_{16}–H_{16}···O_2	0.93	2.58	2.999	108.18
C–H···π	*C*–H	H··· π	C··· π	<(C–H··· π)°
C_{16}–H_{16}···Cg_1	0.96	2.89	3.067(10)	92

Symmetry codes: (i) $-x$, $y+1/2$, $-z+1/2$; (ii) $-x$, $-y+1$, $-z$; (iii) x, $y+1$, z

A stacked FTIR spectrum of the H_2L ligand and MoO_2L·DMF complex is presented in the form of Fig. 5. The two most important absorption peaks visible in the vibrational spectrum of the ligand at 3624 and 1639 cm^{-1} are attributed to the stretching vibration of ν(NH) and ν(C=O). These characteristic peaks disappeared on complexation with molybdenum, which indicate the dianionic nature as well as the sites of coordination of the ligand with metal. The absorption peak of the azomethine chromophore (HC=N) in the spectra of the H_2L ligand and Mo complex appeared at 1602 and 1604 cm^{-1}, respectively. The same pattern of shifting of the stretching vibrational peak of the phenolic oxygen of ligand from 1269 to 1261 cm^{-1} was also perceived [32] to prove the tridentate nature of the ligand. This proclamation is further

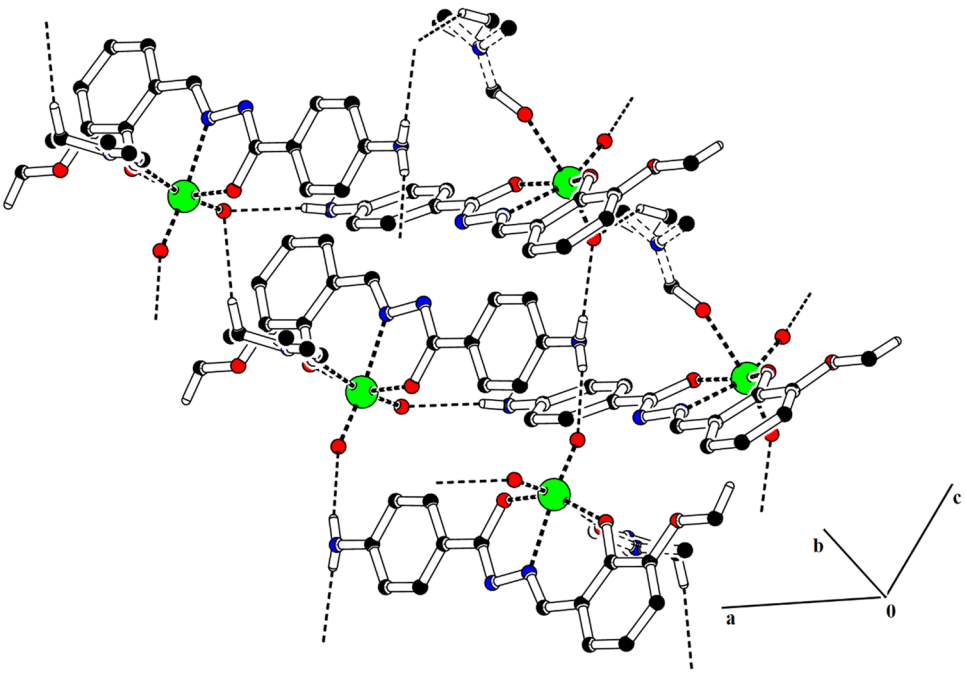

Fig. 3 Packing diagram of MoO_2L·DMF. Only selected H-atoms are shown for clarity

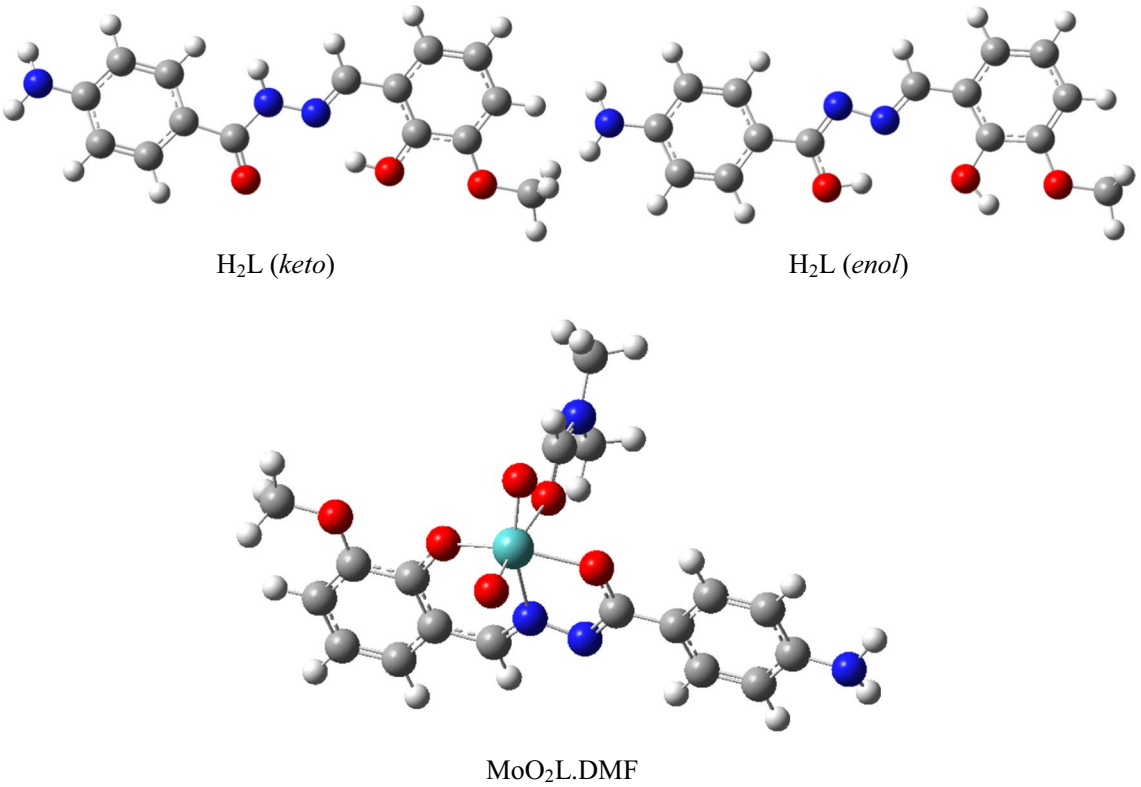

Fig. 4 Optimized structures for H_2L ligand and MoO_2L·DMF complex at the B3LYP/Def2-TZVP level of theory

Table 4 Sum of the electronic and the zero-point energy (E^{ZPE}), enthalpy (H), and Gibbs free energy (G) of the ligand. All values are in Hartree unit

	H_2L (*keto*)		H_2L (*enol*)	
	Gas phase	Solution phase	Gas phase	Solution phase
E^{ZPE}	−970.631	−970.654	−970.620	−970.636
H	−970.611	−970.629	−970.600	−970.611
G	−970.680	−970.712	−970.669	−970.696

1 Hartree = 627.5095 kcal·mol^{-1}

supported by the data obtained in the light of SC-XRD analysis. The distinctive peaks of primary amine (NH_2) in the spectrum of ligand at 3360 and 3441 cm^{-1} were marginally shifted to 3361 and 3466 cm^{-1} in MoO_2L·DMF complex. Cis-$Mo(O)_2$ fraction also gives its symmetric and asymmetric stretching vibrations bands at 912 and 935 cm^{-1} which are in accordance with the literature [32]. Moreover, some new Mo–O and Mo–N peaks are also visible at 590 and 466 cm^{-1} for Mo complex, which are also in agreement to the similar complexes reported earlier. The emergence of shoulder peak around 1651 cm^{-1} for C=O band indicates that the sixth coordination site is occupied by DMF. In addition to this, some new O=Mo–O_{DMF} peaks are also visible at 898 and 831 cm^{-1} for Mo complex [33].

An evaluation of calculated FTIR results of the keto and enol forms of the H_2L ligand and the MoO_2L·DMF complex in the gas phase is shown in the form of stacked spectra in Fig. 6. As evident from the comparison of spectra obtained from experimental and theoretical form, there is a close correspondence in the structure of keto form of H_2L and its Mo complex both in gas and solid states. The theoretical values, 1613 and 1602 cm^{-1}, of vibrational data for azomethine chromophore for both of the synthesized compounds are related to experimental findings (1602 and 1604 cm^{-1}).

While in the case of N–H stretching vibrational frequency values in theoretical (3400 cm^{-1}) and experimental data (3624 cm^{-1}) are far apart from each other. The same set of patterns is manifested in the illustration of C=O stretching frequency where theoretical value was appeared at 1683 cm^{-1}, which is away from the experimental data (1639 cm^{-1}). The difference in the values of vibrational frequencies is due to the involvement of these groups (N–H and C=O) in the hydrogen bonding in solid state.

The ^{1}H and ^{13}C NMR data of the H_2L ligand and its Mo complex in DMSO are presented in the experimental section and the spectra are shown in Figs. 7, 8 and 9. Two signals appearing at $\delta = 11.73$ and 11.33 ppm in the ^{1}H NMR

Table 5 The Mulliken atomic charges of the H_2L ligand and MoO_2L·DMF complex calculated by B3LYP/Def2-TZVP method

Atom	H_2L (*keto*)	H_2L (*enol*)	MoO_2L·DMF	Atom	H_2L (*keto*)	H_2L (*enol*)	MoO_2L·DMF
M_1	–	–	1.456	C_5	−0.198	−0.180	−0.236
O_1	−0.370	−0.380	−0.533	C_6	0.095	0.160	0.096
O_2	−0.341	−0.406	−0.528	C_7	−0.204	−0.201	−0.206
O_3	−0.252	−0.345	−0.255	C_8	−0.018	−0.118	−0.006
O_4	–	–	−0.587	C_9	0.280	0.276	0.417
O_5	–	–	−0.522	C_{10}	0.080	0.055	0.046
O_6	–	–	−0.425	C_{11}	−0.200	−0.184	−0.194
N_1	−0.156	−0.140	−0.064	C_{12}	−0.212	−0.183	−0.183
N_2	−0.176	−0.196	−0.255	C_{13}	0.289	0.293	0.296
N_3	−0.440	−0.443	−0.441	C_{14}	−0.176	−0.182	−0.186
N_4A	–	–	−0.069	C_{15}	−0.184	−0.188	−0.186
C_1	0.150	0.088	0.311	C_{16}	–	–	0.252
C_2	0.199	0.297	0.242	$C_{17}A$	–	–	−0.277
C_3	−0.217	−0.211	−0.234	$C_{18}A$	–	–	−0.244
C_4	−0.151	−0.152	−0.125				

Table 6 A brief overview of experimental and calculated FTIR vibrational parameters (cm^{-1}) of the H_2L ligand and MoO_2L·DMF complex

Assignment	H_2L			MoO_2L·DMF		
	Exp.	Calc. (scaled)[a]	Relative error (%)[b]	Exp.	Calc. (scaled)[a]	Relative error (%)[b]
NH	3624	3400	−6.18	–	–	–
C=O	1639	1683	2.68	–	–	–
–HC=N	1602	1613	0.69	1604	1602	−0.12
C=C	1556	1552	−0.26	1544	1557	0.84
	1475	1459	−1.08	1436	1452	1.11
C–O	1269	1263	−0.47	1261	1259	−0.16
Mo=O	–	–	–	935	973	4.06
				912	937	2.74
Mo–O	–	–	–	590	586	−0.68
Mo–N	–	–	–	466	484	3.86

[a]Scaling factor, 0.965[31]

[b]Relative error (%) $= (X^{Calc} - X^{Exp}) * 100 / X^{Exp}$

spectrum of ligand correspond to OH (phenolic) and NH protons, respectively, disappear on treatment with Mo salt demonstrate about the sites of coordination of the ligand with the molybdenum. This also ascertains the occurrence of keto-imine tautomerism upon complexation. Moreover, a singlet of azomethine proton (–HC=N) at $\delta = 8.56$ ppm observed in the spectrum of the ligand was shifted downfield at $\delta = 8.76$ ppm showing the deshielding due to the decrease in the electronic density upon the coordination of azomethine nitrogen with the metal atom. This is in accordance with the FTIR spectra of complex, where ν(HC=N) appears at higher wavenumber in comparison with the corresponding ligand. There is a slight shift in the positions of aromatic protons in the NMR spectra of the ligand upon complex formation. A singlet of amino proton ($–NH_2$) at $\delta = 5.88$ ppm observed in the spectrum of the ligand was shifted downfield at $\delta = 5.96$ ppm showing the deshielding upon complex formation. The methoxy part of the ligand gives a singlet at $\delta = 3.81$ ppm. These protons are failed to exhibit any noticeable shifts in their positions upon complexation.

The ^{13}C NMR spectra of the ligand and its Mo complex are shown in Fig. 9. The signals for the carbonyl, phenolic and methine carbon were observed at 162.7, 152.4 and 147.0 ppm, respectively.

The chemical shift values of the carbons present in vicinity of the coordinating atoms (i.e., C_9, C_1 and C_8) showed appreciable change in their position due to coordination-induced shifts confirming the association of these functionalities in coordination. The other aromatic carbon atoms of the ligand and the Mo complex appeared in their respective regions according to the literature. Hence, ^{13}C NMR spectra also support the conclusions made from ^{1}H NMR spectral data. The experimental and calculated ^{1}H and ^{13}C NMR chemical shifts of the ligand and its Mo complex are given

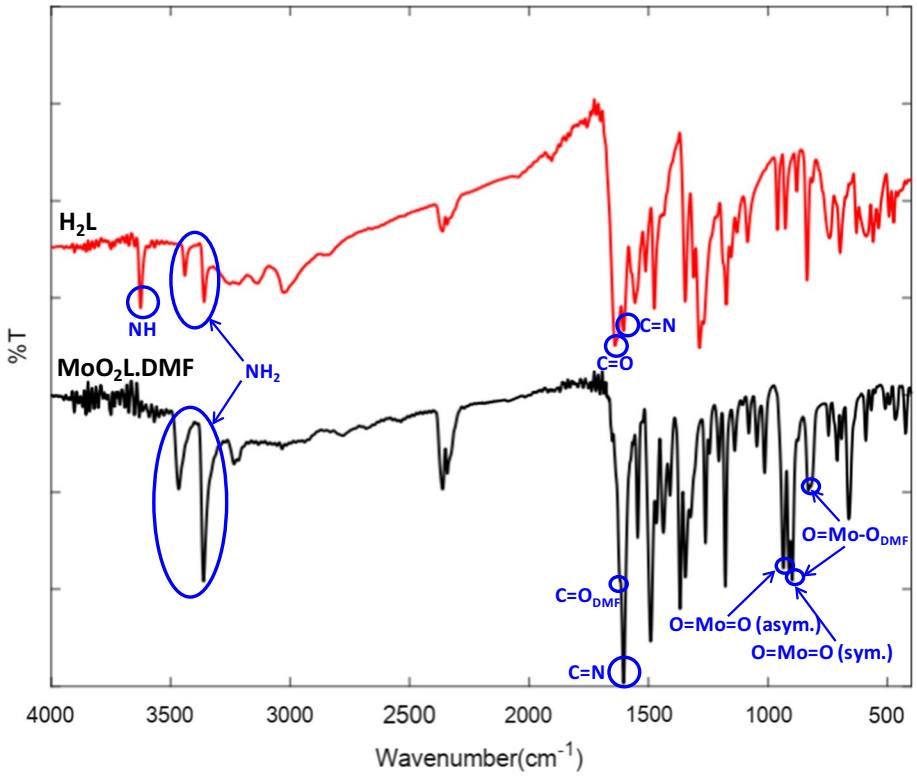

Fig. 5 The experimental FTIR spectra of the H_2L ligand and $MoO_2L{\cdot}DMF$ complex

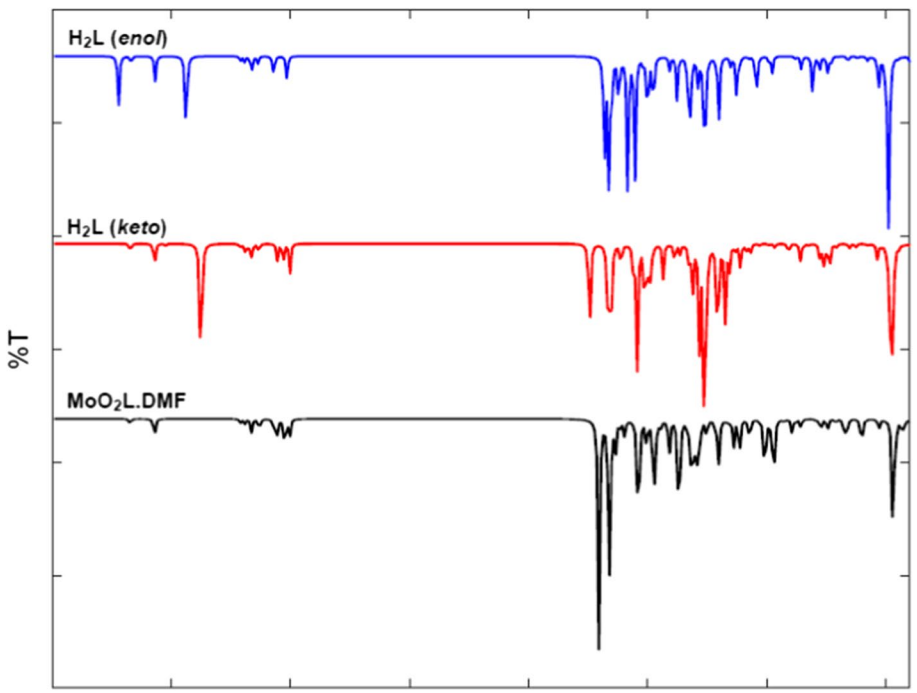

Fig. 6 The theoretical FTIR spectra of H_2L (enol and keto) and $MoO_2L{\cdot}DMF$

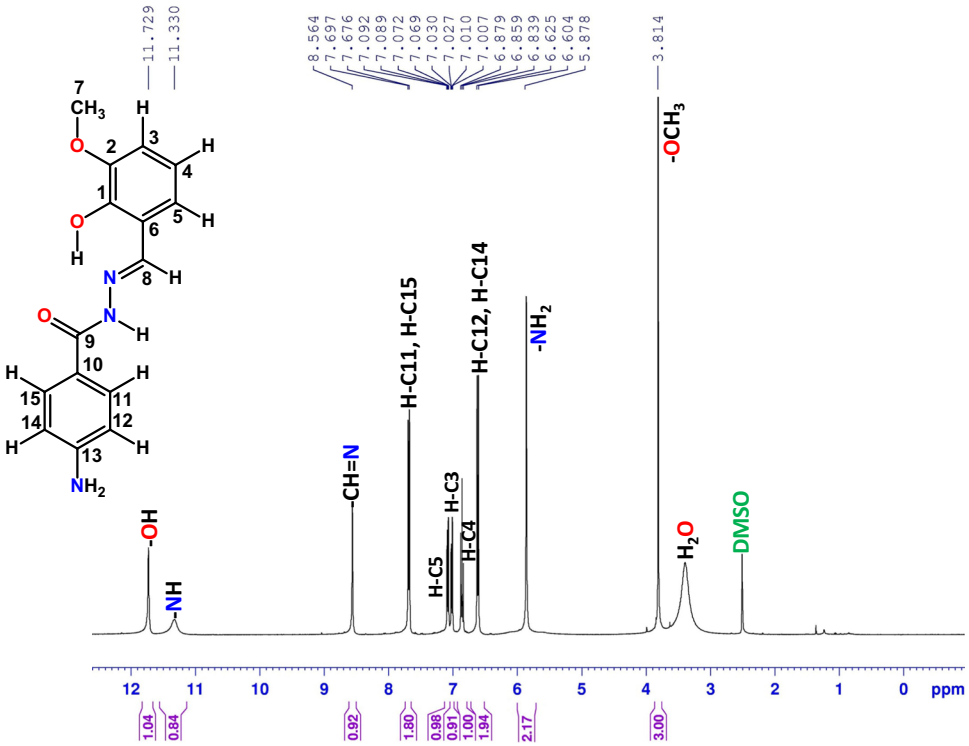

Fig. 7 ^{1}H NMR spectrum of the H_2L ligand in DMSO-d_6

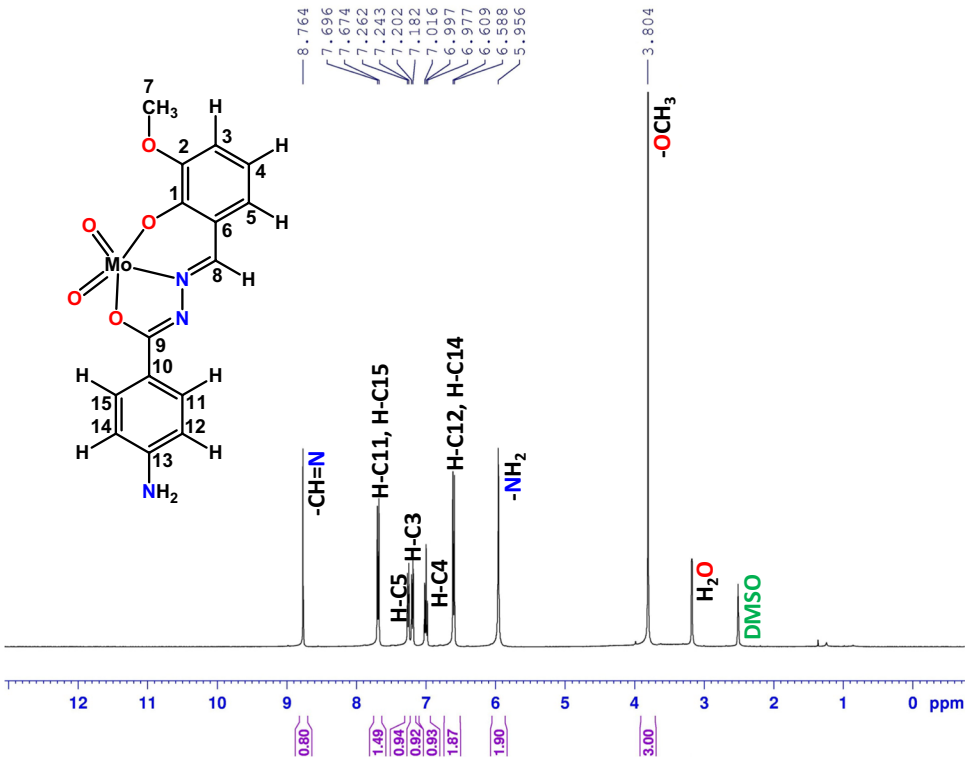

Fig. 8 ^{1}H NMR spectrum of the Mo complex in DMSO-d_6

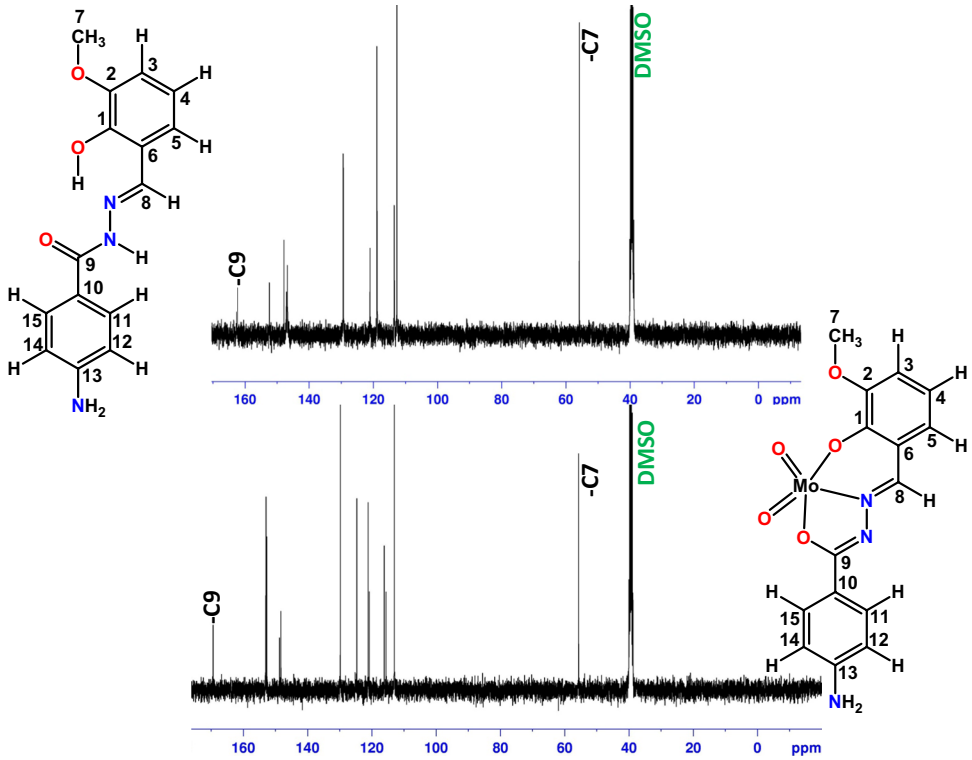

Fig. 9 ^{13}C NMR spectra of the H_2L ligand and Mo complex in DMSO-d_6

Table 7 Experimental and calculated ^{1}H and ^{13}C NMR shifts of ligand and Mo complex (ppm)

Protons	^{1}H NMR				Carbons	^{13}C NMR			
	H_2L		MoO_2L			H_2L		MoO_2L	
	Exp.	Calc.	Exp.	Calc.		Exp.	Calc.	Exp.	Calc.
OH	11.73	12.02	–	–	C_9	162.7	168.9	169.4	177.9
NH	11.33	9.09	–	–	C_{13}	152.4	161.0	152.6	160.9
HC=N	8.56	8.43	8.76	8.82	C_1	147.8	158.4	148.4	157.4
CH(15)	7.68	8.27	7.68	7.99	C_2	147.0	157.3	148.8	157.8
CH(11)		7.82		8.40	C_8	146.8	153.3	153.0	160.4
CH(5)	7.07	7.21	7.25	7.36	C_{15}	129.4	138.7	129.9	138.0
CH(3)	7.02	7.20	7.19	7.29	C_{11}		134.2		138.3
CH(4)	6.88	7.22	6.99	7.33	C_5	121.3	128.3	124.7	131.3
CH(14)	6.61	7.01	6.60	6.89	C_{10}	121.0	126.6	121.2	123.5
CH(12)		6.92		6.93	C_6	119.0	125.1	120.8	127.6
NH_2	5.88	4.05*	5.96	4.07*	C_4	118.7	124.3	116.2	127.8
$CH_3(7)$	3.81	3.97*	3.80	3.92*	C_3	113.5	119.1	115.6	121.1
					C_{14}	112.7	117.7	113.1	118.0
					C_{12}		117.5		118.8
					C_7	55.7	58.6	55.7	59.0

*Average values obtained from calculations

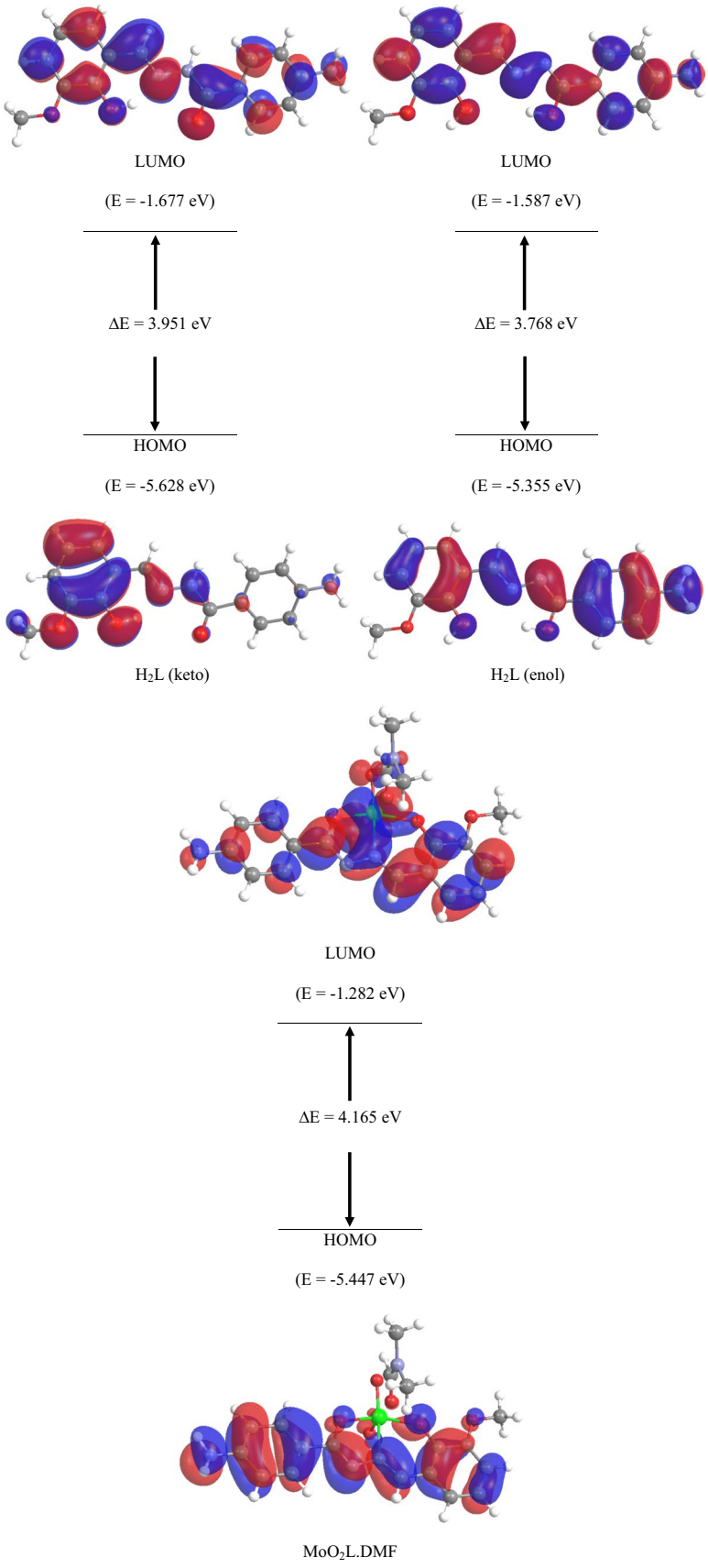

Fig. 10 DFT-optimized frontier molecular orbitals for H_2L ligand (keto and enol) and $MoO_2L{\cdot}DMF$ complex

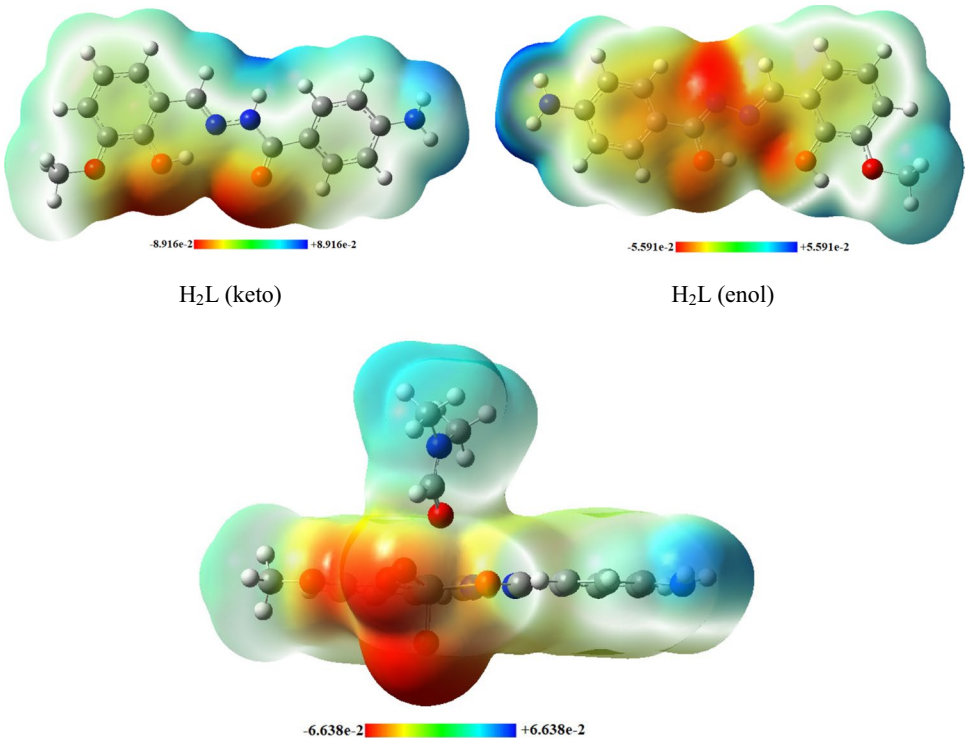

H_2L (keto) H_2L (enol)

MoO_2L.DMF

Fig. 11 Molecular electrostatic potential (MEP) for H_2L ligand (keto and enol) and MoO_2L·DMF complex with color range along with scale

in Table 7. It is obvious from the table that the theoretical data are in close agreement with the experimental findings.

The energy gap ($E_{LUMO} - E_{HOMO}$) is an important factor that helps to determine the kinetic stability and chemical reactivity of the molecule. The stability of the compound increases with the increase in the size of the energy gap. On the other hand, as the energy gap decreases, the reactivity increases and the amount of electronic charge transfer from the ligand to the central metal atom also increases, i.e., it easily offers electrons to an acceptor. The energy of the frontier HOMO and LUMO and their energy gaps (ΔE) for the H_2L ligand and MoO_2L·DMF complex were computed by DFT at the B3LYP/Def2-TZVP level of theory. The results are shown in Fig. 10. The energy gaps for the H_2L (keto), H_2L (enol) and MoO_2L·DMF were found to be 3.951, 3.768 and 4.165 eV, respectively. As it turns out, the keto form of the ligand is more stable than the enol form owing to its higher energy gap.

Molecular electrostatic potential (MEP) analysis provides information about the reactive sites of the molecules. The MEP can show positive regions (marked in blue) related to nucleophilic attack and negative regions (marked in red) relevant to electrophilic reactivity. The molecular electrostatic potential of the H_2L ligand in both keto and enol tautomeric forms and the MoO_2L·DMF complex was calculated and shown in Fig. 11, along with the values of electrostatic potentials. Theoretically, the electron-rich regions around the oxygen atoms of hydroxyl and carbonyl groups are potentially active sites of the ligand toward positively charged metal. These results are in agreement with the Mulliken atomic charges (Table 5).

Theoretical calculations confirm the results obtained from the experimental analysis that the metal atom coordinated to the Schiff base ligand via the azomethine nitrogen atom (N_1), the oxygen of the deprotonated hydroxyl group (O_1)

Table 8 Effect of the catalyst amount, oxidant, solvent and temperature on the selective oxidation of 4-chlorobenzyl alcohol using MoO_2L·DMF complex[a]

Entry	Oxidant	Catalyst (mmol)	Solvent	Condition	Time (h)	Yield (%)
1	No oxidant	0.006	MeCN	Reflux	3	Trace
2	*tert*-BuOOH	0.006	MeCN	Reflux	3	50
3	$(Bu)_4NIO_4$	0.006	MeCN	Reflux	3	10
4	$NaIO_4$	0.006	MeCN	Reflux	3	25
5	H_2O_2	0.006	MeCN	Reflux	3	50
6	UHP	0.006	MeCN	Reflux	2	91
7	UHP	–	MeCN	Reflux	2	Trace
8	UHP	0.004	MeCN	Reflux	2	65
9	UHP	0.008	MeCN	Reflux	2	92
10	UHP	0.006	MeOH	Reflux	2	55
11	UHP	0.006	EtOH	Reflux	2	40
12	UHP	0.006	1,2-DCE	Reflux	2	20
13	UHP	0.006	Acetone	Reflux	2	55
14	UHP	0.006	$CHCl_3$	Reflux	2	20
15	UHP	0.006	CCl_4	Reflux	2	Trace
16	UHP	0.006	CH_2Cl_2	Reflux	2	Trace
17	UHP	0.006	MeCN	r.t	2	Trace
18	UHP	0.006	MeCN	50 °C	2	45
19	UHP	0.006	MeCN	70 °C	2	80

[a]Reaction conditions: 4-chlorobenzyl alcohol (1 mmol), oxidant (2 mmol), catalyst, solvent (10 mL) under different temperatures

and the oxygen of carbonyl group (O_3) and hence, the ligand behaves in a tridentate fashion.

Catalytic oxidation results

Dioxomolybdenum complexes often show interesting catalytic properties, especially in oxidation reactions [34]. Compared to previously reported species, the present complex has excellent activity and selectivity. The catalytic activity of MoO_2L·DMF complex was explored by the selective oxidation of benzylic alcohols to benzaldehydes.

In order to optimize the catalytic system, including the MoO_2L·DMF complex as catalyst and UHP (2 mmol) as oxidant, the oxidation of 4-chlorobenzyl alcohol (1 mmol) was chosen as a model reaction, and the influence of different factors, that may affect the reaction, were investigated (Table 8). Various oxidants were tested (Entries 2–6), and the results showed that the UHP is the best oxygen source in this reaction. Different amounts of the catalyst were used (Entries 6–9) and it was observed that in the absence of the catalyst the reaction failed to proceed. The rate of conversion was increased with the increase in the amount of catalyst and complete transformation was observed when 0.006 mmol of Mo complex was used. The activity of the catalytic system was examined in various solvents under reflux conditions (Entries 6, 10–16) and it was found that acetonitrile is the best solvent for the reaction. Finally, by changing the reaction temperature, the catalytic oxidation reaction of 4-chlorobenzyl alcohol in the presence of MoO_2L·DMF complex in acetonitrile was performed (Entries 6, 17–19). It is obvious that the rate of reaction increases with the increase in temperature and the best result was spotted under reflux conditions.

Selective oxidation of various substituted benzylic alcohols was evaluated under the optimized reaction conditions (Table 9). As shown in Table 9, a variety of benzylic

Table 9 Selective oxidation of benzylic alcohols to benzaldehydes with UHP catalyzed by MoO_2L·DMF complex[a]

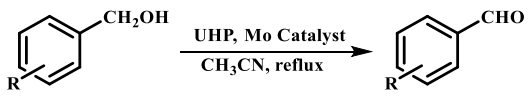

Entry	Alcohol	Aldehyde[b,c]	Time (h)	Yield (%)
1	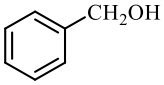	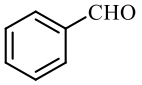	2	92
2	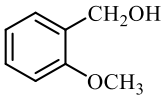	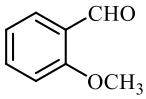	2.5	91
3	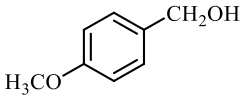	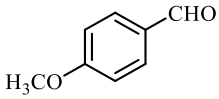	2	88
4	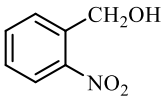	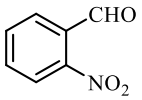	2.5	90
5	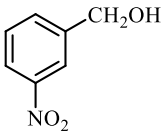	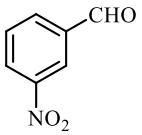	2.5	89
6	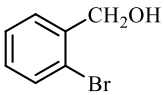	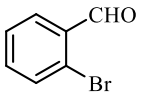	2	90
7	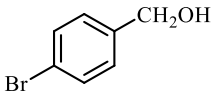	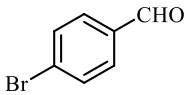	2.5	90
8	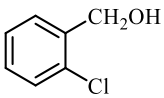	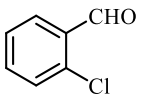	2	88
9	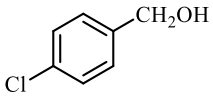	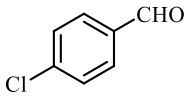	2	91
10	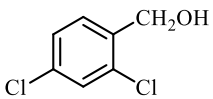	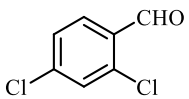	3	89

[a]Reaction conditions: benzylic alcohol (1 mmol), UHP (2 mmol), catalyst (0.006 mmol), CH_3CN (10 mL) under reflux conditions

[b]All products were identified by the comparison of their physical and spectral data with those of authentic samples

[c]Isolated yield

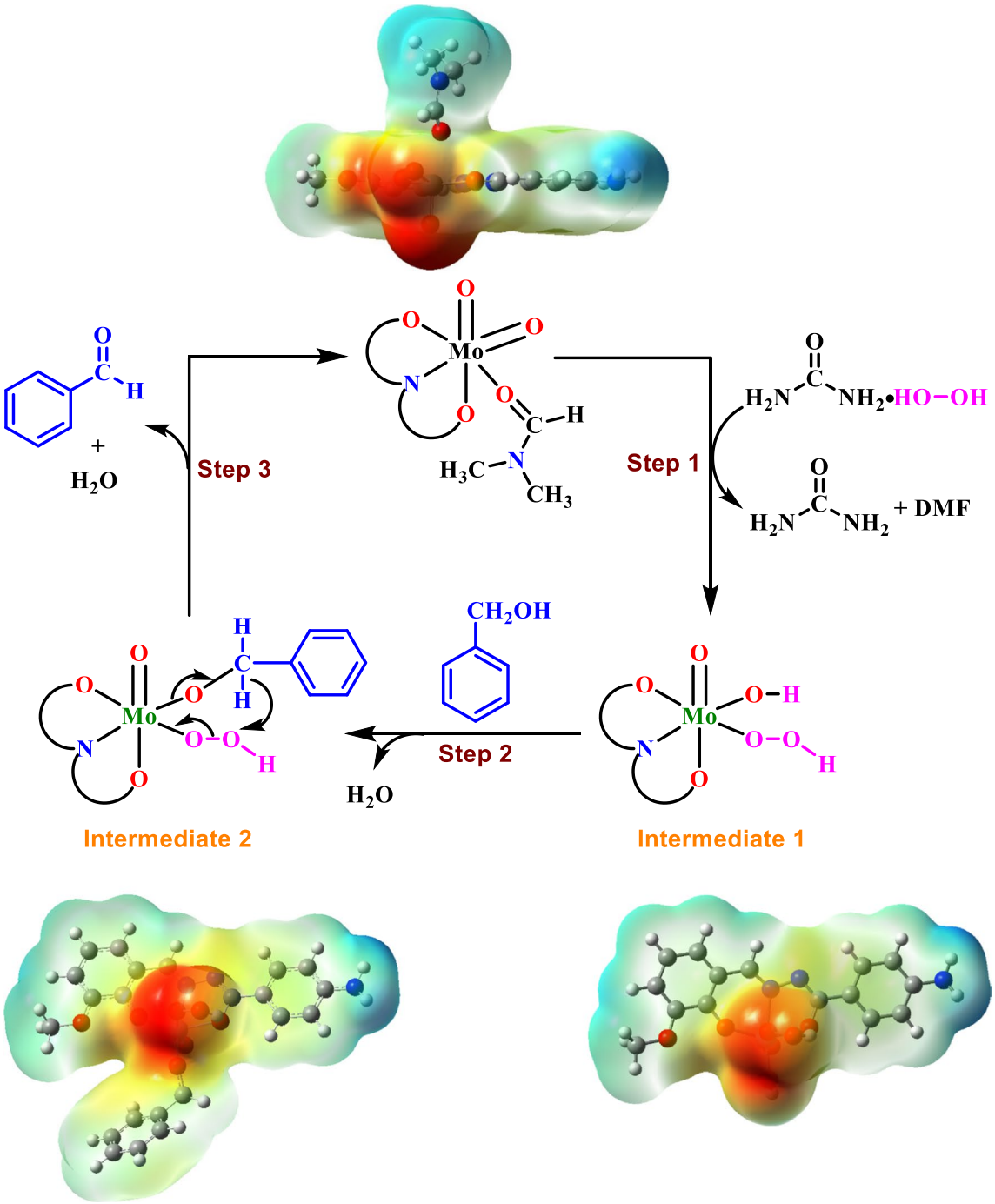

Scheme 3 Plausible mechanism for oxidation of benzyl alcohol with UHP catalyzed by MoO_2L·DMF complex

alcohols, with both electron-donating and electron-withdrawing groups, are treated with UHP to give the corresponding substituted benzaldehydes in excellent yields. The chemoselectivity of the procedure was remarkable. The alcohols were oxidized under the affection of this catalytic system, and the desired aldehydes were obtained in 100% selectivity. The most important advantage of this method is that there is no evidence of overoxidation to the production of carboxylic acid in all substrates.

According to experimental findings and information found in relevant literature [4], for the oxidation reactions mediated by oxometal complexes, a plausible mechanism

Table 10 Sum of the electronic and the zero-point energy (E^{ZPE}), enthalpy (H), and Gibbs free energy of all the materials involved in the oxidation of benzyl alcohol catalyzed by MoO_2L·DMF complex in the refluxed acetonitrile

Compound	E^{ZPE}	H	G
MoO_2L·DMF	− 1188.393	− 1188.362	− 1188.459
Intermediate 1	− 1339.969	− 1339.933	− 1340.040
Intermediate 2	− 1610.312	− 1610.269	− 1610.399
Benzyl alcohol	− 346.786	− 346.775	− 346.826
H_2O_2	− 151.599	− 151.594	− 151.627
Benzaldehyde	− 345.605	− 345.595	− 345.643
H_2O	− 76.449	− 76.445	− 76.471

All values are listed in Hartree unit[a]

[a]1 Hartree = 627.5095 kcal.mol^{-1}

Table 11 The changes of the electronic and the zero-point energy (ΔE^{ZPE}), enthalpy (ΔH), and Gibbs free energy (ΔG) of all the reaction steps in the oxidation of benzyl alcohol catalyzed by MoO_2L·DMF complex in the refluxed acetonitrile

	ΔE^{ZPE}		ΔH		ΔG	
	Hartree	kcal·mol^{-1}	Hartree	kcal·mol^{-1}	Hartree	kcal·mol^{-1}
Step 1	0.023	14.43	0.023	14.43	0.046	28.87
Step 2	− 0.007	− 4.39	− 0.006	− 3.77	− 0.004	− 2.51
Step 3	− 0.135	− 84.71	− 0.133	− 83.46	− 0.174	− 109.19

1 Hartree = 627.5095 kcal.mol^{-1}

for oxidation of benzyl alcohol using UHP catalyzed by MoO_2L·DMF complex is proposed and depicted in Scheme 3. The homogeneous catalyst, MoO_2L·DMF, is inactive without the assistance of UHP in the oxidation process. As shown in the MEP diagram of MoO_2L·DMF and also it was previously explained that the metal atom in the complex is electropositive and can be attacked by a nucleophile. Thus, the MoO_2L·DMF complex reacts with a hydrogen peroxide molecule released from UHP to form the peroxo molybdenum species (Intermediate 1). This peroxo molybdenum intermediate is active in oxidation and after etherification by benzyl alcohol generates intermediate 2 and a molecule of water was produced in lieu of by-product. Ultimately, intermediate 2 also releases a water molecule and gives benzaldehyde as the target product and regenerates the MoO_2L·DMF Schiff base complex.

The sum of the electronic and the zero-point energy (E^{ZPE}), enthalpy (H), and Gibbs free energy (G) of all the materials involved in the selective oxidation of benzyl alcohol to benzaldehyde using UHP in the presence of MoO_2L·DMF catalyst are listed in Table 10. By use of these values, ΔE^{ZPE}, ΔH and ΔG of all steps for this reaction were calculated and presented in Table 11. As shown in Table 11, the first step of the reaction is endothermic ($\Delta G = 28.87$ kcal·mol^{-1}) and can be carried out at 82 °C. The second and the last step of the reaction is exothermic with $\Delta G = -2.51$ and -109.19 kcal·mol^{-1}, respectively, and overall, the reaction is exothermic.

Conclusion

In the current research work, we have synthesized a new tridentate ONO-donor Schiff base ligand and its Mo(VI) complex and characterized them by various physicochemical techniques. Theoretical calculations of the Schiff base ligand and its Mo complex were performed using DFT at B3LYP/Def2-TZVP level of theory. The results showed that the theoretical data are in good consensus with the experimental outcomes. The catalytic activity of the complex was also investigated for the selective oxidation of benzylic alcohols to benzaldehydes by using UHP in acetonitrile under reflux conditions. This method has numerous ascendancies such as high yield, short reaction time and excellent selectivity to produce corresponding benzaldehydes without overoxidation to benzoic acids.

Supplementary materials

Crystallographic data for the structural analysis have been deposited with the Cambridge Crystallographic Data Centre as supplementary publication no. CCDC 2,059,956 for the molybdenum complex. Copies of this information may be obtained free of charge via http://www.ccdc.cam.ac.uk/conts/retrieving.html or from The Director, CCDC, 12 Union Road, Cambridge, CB2 1EZ, UK.

Acknowledgements We gratefully acknowledge practical support of this study by Ardakan University and Payame Noor University.

Declarations

Conflict of interest No potential conflict of interest was reported by the authors.

References

1. Wang Q, Xiong ZD, Liu L, Cai YJ (2021) Syntheses, X-ray crystal structures and catalytic epoxidation of oxidovanadium(V) and dioxidomolybdenum(VI) complexes derived from N′-(4-Bromo-2-hydroxybenzylidene)benzohydrazide. Inorg Nano-Met Chem 51:12–19
2. Cardona F, Parmeggiani C (2014) Transition metal catalysis in aerobic alcohol oxidation, pp 1–39
3. Kroschwitz JI, Othmer K (1992) Encyclopedia of chemical technology. Wiley, New York, pp 64–72

4. Hatefi-Ardakani M, Saeednia S, Pakdin-Parizi Z, Rafeezadeh M (2016) Efficient and selective oxidation of alcohols with tert-BuOOH catalyzed by a dioxomolybdenum(VI) Schiff base complex under organic solvent-free conditions. Res Chem Intermed 42:7223–7230
5. Roztocki K, Senkovska I, Kaskel S, Matoga D (2016) Carboxylate–hydrazone mixed-linker metal–organic frameworks: Synthesis, structure, and selective gas adsorption. Eur J Inorg Chem 4450–4456
6. Aboafia SA, Elsayed SA, El-Sayed AK, El-Hendawy AM (2018) New transition metal complexes of 2,4-dihydroxybenzaldehyde benzoylhydrazone Schiff base (H2dhbh): synthesis, spectroscopic characterization, DNA binding/cleavage and antioxidant activity. J Mol Struct 1158:39–50
7. Maurya MR, Haldar C, Kumar A, Kuznetsov ML, Avecilla F, Pessoa JC (2013) Vanadium complexes having [VO]2+, [VO]3+ and [VO2]+ cores with hydrazones of 2,6-diformyl-4-methylphenol: synthesis, characterization, reactivity, and catalytic potential. Dalton Trans 42:11941–11962
8. Kuhn FE, Santos AM, Abrantes M (2016) Effective homogeneous molybdenum catalyst for linear terminal alkenes epoxidation with organic hydroperoxide. Chem Rev 106:2455–2475
9. Martos Calvente R, Campos-Martin JM, Fierro JLG (2002) Effective homogeneous molybdenum catalyst for linear terminal alkenes epoxidation with organic hydroperoxide. Catal Commun 3:247–251
10. Abu-omar MM, Loaiza A, Hontzeas N (2005) Reaction mechanisms of mononuclear non-heme iron oxygenases. Chem Rev 105:2227–2252
11. Saheb V, Sheikhshoaie I, Stoeckli-Evans H (2012) A novel tridentate Schiff base dioxo-molybdenum(VI) complex: synthesis, experimental and theoretical studies on its crystal structure, FTIR, UV–visible, 1H NMR and 13C NMR spectra. Spectrochim Acta A Mol Biomol Spectrosc 95:29–36
12. Cindrić M, Pavlović G, Katava R, Agustin D (2017) Towards a global greener process: from solvent-less synthesis of molybdenum (VI) ONO Schiff base complexes to catalyzed olefin epoxidation under organic-solvent-free conditions. New J Chem 41:594–602
13. Sheikhshoaie I, Rezaeifard A, Monadi N, Kaafi S (2009) A novel tridentate Schiff base dioxo-molybdenum(VI) complex: synthesis, crystal structure and catalytic performance in green oxidation of sulfides by urea hydrogen peroxide. Polyhedron 28:733–738
14. Kaicharla T, Yetra SR, Roy T, Biju AT (2013) Engaging isatins in solvent-free, sterically congested Passerini reaction. Green Chem 15:1608–1614
15. İlhan-Ceylan B, Bolukbasi O, Yilmaz A, Kaya K, Kurt Y, Ülküseven B (2021) Synthesis, spectroscopic characterization and quantum chemical studies of a dioxomolybdenum (VI) complex with an N,S-substituted pyridoxal thiosemicarbazone. Polyhedron 193:114884
16. Lorber CY, Smidt SP, Osborn JA (2000) Selective and environmentally benign aerobic catalytic oxidation of alcohols by a molybdenum-copper system. Eur J Inorg Chem 4:655–658
17. Kargar H, Aghaei-Meybodi F, Behjatmanesh-Ardakani R, Elahifard MR, Torabi V, Fallah-Mehrjardi M, Tahir MN, Ashfaq M, Munawar KS (2021) Synthesis, crystal structure, theoretical calculation, spectroscopic and antibacterial activity studies of copper(II) complexes bearing bidentate Schiff base ligands derived from 4-aminoantipyrine: influence of substitutions on antibacterial activity. J Mol Struct 1230:129908
18. Bruker (2012) APEX2, Bruker AXS Inc, Madison, Wisconsin, USA
19. Sheldrick GM (2002) SADABS, Version 2.03, University of Göttingen, Germany
20. Sheldrick GM (1997) In: SHELXS97 and SHELXL97, University of Göttingen, Germany, pp 1600–5368
21. Sheldrick GM (2015) Crystal structure refinement with SHELXL. Acta Crystall Sec C71:3–8
22. Farrugia LJ (2012) WinGX and ORTEP for windows: an update. J App Crystallogr 45:849–854
23. Spek AL (2009) Structure validation in chemical crystallography. Acta Crystall Sec D Biol Crystallogr 65:148–155
24. Macrae CF, Sovago I, Cottrell SJ, Galek PTA, McCabe P, Pidcock E, Platings M, Shields GP, Stevens SJ, Towler M, Wood PA (2020) Mercury 4: from visualization to analysis, design and prediction. J Appl Cryst 53:226–235
25. Frisch MJ, Trucks GW, Schlegel HB, Scuseria GE, Robb MA, Cheeseman JR, et al (2013) GAUSSIAN 09 (Revision D.01), Gaussian, Inc., Wallingford, CT
26. Becke AD (1993) Quantum mechanical continuum solvation models. J Chem Phys 98:5648–5652
27. Tomasi J, Mennucci B, Cammi R (2005) Quantum mechanical continuum solvation models. Chem Rev 105:2999–3093
28. Weigend F, Ahlrichs R (2005) Balanced basis sets of split valence, triple zeta valence and quadruple zeta valence quality for H to Rn: design and assessment of accuracy. Phys Chem Phys 7:3297–3305
29. Gauss J (1993) Effects of electron correlation in the calculation of nuclear magnetic resonance chemical shifts. J Chem Phys 99:3629–3643
30. http://www.chemissian.com
31. Palafox MA (2018) Analogue simulation with the use of artificial quantum coherent structures. Phys Sci Rev 3:1–30
32. Shebl M (2008) Synthesis and spectroscopic studies of binuclear metal complexes of a tetradentate N_2O_2 Schiff base ligand derived from 4,6-diacetylresorcinol and benzylamine. Spectrochim Acta A Mol Biomol Spectrosc 70:850–885
33. Cvijanovic D, Pisk J, Pavlovic G, Sisak-Jung D, Matkovic-Calogovic D, Cindric M, Agustin D, Vrdoljak V (2019) Discrete mononuclear and dinuclear compounds containing a MoO 22+ core and 4-aminobenzhydrazone ligands: synthesis, structure and organic-solvent-free epoxidation activity. New J Chem 43:1791–1802
34. Karman M, Wera M, Romanowski G (2020) Chiral cis-dioxidomolybdenum (VI) complexes with Schiff bases possessing two alkoxide groups: synthesis, structure, spectroscopic studies and their catalytic activity in sulfoxidation and epoxidation. Polyhedron 187:114653